Structural characterization and electrochemical properties of non-graphitizable carbons for a lithium ion battery

Katsuhisa Tokumitsu *, Hiroyuki Fujimoto, Akihiro Mabuchi, Takahiro Kasuh

Research and Development Center, Osaka Gas Co. Ltd., 6-19-9, Torishima, Konohana-ku Osaka 554-0051, Japan

Abstract

Structural characteristics and electrochemical properties of non-graphitizable carbons were investigated. The carbons were obtained by heat-treating the oxidized graphitizable carbon precursors with various molar ratios of aromatic compounds and cross-linking agent. The discharge profiles of the non-graphitizable carbons heat-treated at 600°C had one plateau discharge region at 1.0 V vs. Li/Li$^+$, which is similar to graphitizable ones heat-treated at the temperature. However, the discharge profiles of the non-graphitizable carbons heat-treated above 800°C exhibited two plateau discharge regions at 0.2 and 1.0 V vs. Li/Li$^+$. The discharge capacities of the non-graphitizable carbons increased with an increase of cavity volume, which was controlled by molar ratios of aromatic compound and cross-linking agent. The structural parameters proposed were measured to compare with each other, and it was found that they showed good correlation. © 2000 Elsevier Science S.A. All rights reserved.

Keywords: Lithium ion battery; Lithium insertion; Intercalation compounds; X-ray diffraction; Electrochemical properties

1. Introduction

Lithium ion batteries have recently attracted much attention because of the higher voltage, higher energy density and longer cycle life in comparison with other conventional rechargeable batteries. This interest has been driven largely by the proliferation to satisfy their strong need for lightweight energy sources in the electronic equipment, portable computers, cellular phones, and electric vehicles. When lithium metal is used as an anode, the theoretical specific capacity is 3860 A h kg^{-1}. During charge–discharge cycles, however, it was found that re-deposited lithium formed dendrites on the surface of the lithium metal and that it caused a poor cycle life of a lithium battery. A major advance was made by using carbon materials, which can include lithium species as an ion within the carbon structure [1–5]. When graphitic materials (including natural graphite and other graphitized materials) are used as anode for lithium ion batteries, their theoretical specific capacity is 372 A h kg^{-1}, which corresponds to

the first stage of the lithium intercalated graphite (LiC$_6$). The capacity of graphitic materials is far below that of lithium metal. Carbon materials other than graphitic materials have a variety of structures, which depend strongly on the nature of the carbon precursors, and the heat-treatment conditions. Many efforts have been undertaken to find carbon materials having higher capacity than the theoretical limit. Recently, many kinds of carbon materials having capacities higher than the theoretical value have been obtained by heat-treating polyfurfulyl alcohol [6], polyparaphenylene [7], and phenolic resin [8,9]. In order to explain the capacities of such carbon materials beyond the theoretical value, a number of explanations have been proposed. A mechanism, in which all lithium species including Li$_2$ covalent molecules are intercalated into interlayers to form LiC$_2$, was proposed by Sato et al. [7]. Zheng et al. [10] reported a striking correlation between the capacity and their hydrogen content of a series of carbons. Liu et al. [11] reported that lithium ions can be adsorbed on both sides of the single-layer carbon sheet, to form the ''house of cards'' arrangement, and proposed that the specific capacity could ultimately be twice that of graphite. The authors proposed the R parameter, related to the (002) peak-to-background ratio, which measured the fraction of single graphene sheets in X-ray diffraction

---

* Corresponding author. Fax: +81-66462-3425.
E-mail address: ktokumit@osakagas.co.jp (K. Tokumitsu).

(XRD). Yazami and Deschamps [12] reported a multi-layer mechanism for carbon anodes with high capacities. Matsumura et al. [13] reported that small crystallite size was suitable for high specific capacity. Xiang et al. [14] prepared carbon materials from phenolic resins with different cross-linking densities and found that the edge length of stacking graphene layers, ''EL'', was proportional to the capacity of the plateau at about 1.0 V vs. Li/Li$^+$. In our previous papers, the cavities in the carbon structure are concluded to accommodate lithium species, contributing to the charge–discharge capacity, especially toward the plateau discharge capacity around 1.0 V vs. Li/Li$^+$ [15–18]. In Ref. [18], graphitizable carbons of controlled structure was synthesized from condensed poly-nuclear aromatics (COPNA) resins using pyrene (Py) as an aromatic compound and dimethyl-p-xylene glycol (DMPXG) as a cross-linking agent. The carbon structure of such carbons was controlled by the molar ratios of cross-linking agent to aromatic compound. The increase in the plateau discharge capacities of these carbons around 1.0 V vs. Li/Li$^+$ depended mainly on the volume of cavity in the carbon. This technique, therefore, allows us to systematically change the structure of non-graphitizable, as well as graphitizable carbons by means of selected precursors with controlled molar ratios of the cross-linking agent.

Generally speaking, the difference between graphitizable and non-graphitizable carbons is that graphitizable carbon shows anisotropic texture while non-graphitizable carbon shows isotropic texture under optical microscope observation. According to the structural differences of graphitizable and non-graphitizable carbons, although both these carbons have almost the same charge profiles, the discharge ones of these carbons are different. In other words, non-graphitizable carbons prepared around 1000°C have higher capacities than the theoretical limit, 372 A h kg^{-1}, with a plateau discharge region below 0.2 V vs. Li/Li$^+$. On the other hand, graphitizable carbons prepared under 800°C also have higher capacities than that with a different plateau region around 1.0 V vs. Li/Li$^+$. Zheng et al. [10] reported high-capacity non-graphitizable carbon materials prepared from phenolic and epoxy resins. Xing et al. [19] reported optimized pyrolysis conditions to obtain high-capacity non-graphitizable carbon materials from sugar. Such raw materials are typical precursors for the non-graphitizable carbon materials. Since their structural control is very difficult, the following questions rise inevitably. Do only the non-graphitizable carbons prepared from conventional non-graphitizable precursors have high capacities with a plateau discharge region below 0.2 V vs. Li/Li$^+$? Do non-graphitizable carbons prepared from graphitizable precursors through proper chemical modification also show the same property? Furthermore, can we control the discharge profile and/or the capacity of the non-graphitizable carbon using the cavity control technique by changing the amount of cross-linking agent as succeeded for graphitizable carbons?

Many methods for obtaining a non-graphitizable carbon from a graphitizable carbon precursors have been reported, for example, oxidation (including ozonization) [20,21] or air blowing reaction [22,23] of the precursors, and adding sulfur [24] or nitrobenzene [25] to precursors. Adding sulfur or nitrobenzene to the precursors, however, was not recommended for a carbon anode, because the elements of sulfur or nitrogen still remain in the carbon structure even after heat treatment around 600°C. Oxidative modification of the graphitizable DMPXG/Py precursors appears suitable to obtain the non-graphitizable carbons of well-defined structure.

In this paper, the relationship between the carbon structures and charge–discharge properties of the non-graphitizable carbons was intended, using the graphitizable precursors in the previous paper [18] through the oxidization before carbonization to completely kill their fusibility.

Their structural parameters such as R [11], EL [14], CI [26] were measured to compare the cavity capacity with the observed capacity.

2. Experimental

2.1. Preparation of carbon precursor and carbon materials

The COPNA precursors were synthesized by the reaction of Py and DMPXG, the latter of which functioned as a cross-linking agent at molar ratios of 1.0, 1.5, and 2.0.

The precursors were crushed coarsely by coffee mil (particle diameter < 30 μm) and oxidized at 300°C in air by a heating with a rate of 1°C min^{-1} at a soak time of 2 h and air flow rate of 1 l min^{-1}. Such an oxidizing treatment was repeated two to three times. The oxidized precursors were heat-treated to temperatures of 600°C, 800°C, 1100°C, and 1400°C in a muffle furnace at 2°C min^{-1} and soaked for 2 h.

2.2. XRD measurement

The XRD profiles of the carbons were measured with Cu Kα (Rigaku, RINT-2500). The lattice constant and crystallite size along a-axis were determined referring to an internal standard of Si. Diamond's [27–30] method was applied to estimate the crystallite size, L_a. The fraction of number of layers against the stacking distribution and the average number of layers per stack were calculated based on the Patterson function of the XRD profile on (002) using a Fourier transform (the so-called Hirsch's [31] method). The value of SI was calculated by the (002) intensity which was normalized by the base line intensity around $2\theta \approx 33°$ [32]. The SI value indicates the probability of disturbances in the stacking of the layers in carbon materials.

2.3. TEM observation

TEM observation was carried out at the magnitude of 200 K (JEOL, 1200 EX). The carbon samples were mounted in an epoxy resin which was cured at 60°C for 24 h. The specimen were cut by microtome (Reichert, Ultracut N) into the thickness of 40 nm and placed on the copper mesh (3 mm in diameter).

2.4. Measurement of butanol displacement density

Butanol displacement density was measured at 30°C according to Japanese Industrial Standard R 7212.

2.5. Assessment of the theoretical capacity

The CI value was calculated with the following equation [26]

$$CI = 1 - \frac{D}{D^i} \frac{c_0}{c_0^i} \frac{a_0^2}{a_0^{i2}} \frac{L_c}{L_c + c_0/2} \frac{L_a^2}{(L_a + a_0)^2} \quad (1)$$

where a_0, c_0, L_a, and L_c represent the lattice constants and the crystallite size of the carbon along a- and c-axes, respectively. The value of D denotes the density of carbon. The superscript "i" indicates the parameter of the ideal graphite.

The theoretical capacity, Q_{cavity}, ascribed to the cavity was calculated by the following equation [33]

$$Q_{cavity} = \frac{2F}{NDa_{Li}^3} CI$$

$$= \frac{2F}{NDa_{Li}^3} \left(1 - \frac{D}{D^i} \frac{c_0}{c_0^i} \frac{a_0^2}{a_0^{i2}} \frac{L_c}{L_c + c_0/2} \frac{L_a^2}{(L_a + a_0)^2} \right) \quad (2)$$

where F, N, and a_{Li} is Faraday's constant, Avogadro's number and the lattice constant in BCC structure, respectively.

2.6. Cell assembly and electrochemical measurement

Working electrodes were fabricated by mixing carbons with 4 wt.% binder (Daikin, Daiflon D-1) suspended in distilled water. The paste-like mixture of ca. 1 mg was spread thinly onto a nickel mesh (5 × 5 mm) and pressed at a pressure of 3.9×10^9 Pa. The electrode was dried in vacuum for 6 h at 200°C.

Electrochemical measurements were performed in a glove box at 25°C using a three-electrode test cell made of glass. Lithium metal was used as a counter electrode and reference electrode. The electrolyte used was 1 M $LiClO_4$ in propylene carbonate (PC). All the operations for the cell assembly were carried out in a glove box filled with argon gas where both the moisture and oxygen concentrations were less than 1 ppm.

A constant current density in charge was applied at 1.0 mA cm^{-2} from 2.0 V to 1.0 mV vs. Li/Li$^+$, using a galvanostat/potentiostat (Hokuto Denko, HJ-201B). The total charging time was limited to 12 h. Discharge was carried out at a constant current density of 1.0 mA cm^{-2} in 0–2.0 V vs. Li/Li$^+$. The geometrical surface area of the electrode was 0.5 cm^2.

3. Results

3.1. Structure of non-graphitizable carbons analyzed by TEM and XRD

Fig. 1 shows the TEM images of carbons heat-treated at 2800°C, which were derived from ''non-oxidized precursor'' and ''oxidized precursor'' at a DMPXG/Py molar ratio of 2.0. As can be seen in this figure, the carbon from non-oxidized precursor showed lamella structure with large crystallite size. On the other hand, oxidized precursor heat-treated at 2800°C gave isotropic carbon with small crystallite size. A non-graphitizable carbon material was obtained as expected from the graphitizable carbon precursors through oxidation.

Table 1 lists the characteristics of the carbons heat-treated from 600°C to 1400°C. Obviously, there is a tendency that the precursors with an increase of DMPXG/Py molar ratios gave a carbon material with lower displacement density and larger CI value, which indicate lower crystallinity of the carbon.

Fig. 2 shows Hirsch's analyses of the DMPXG/Py-based non-graphitizable carbons with a series of DMPXG/Py molar ratios heat-treated at 800°C. Although the fractions of layers which consisted of two graphene layers in DMPXG/Py = 1.5 and 2.0 carbons were both 0.78, the fraction in DMPXG/Py = 1.0 carbon was 0.73 and the maximum ''packing number'' was 5. These results indi-
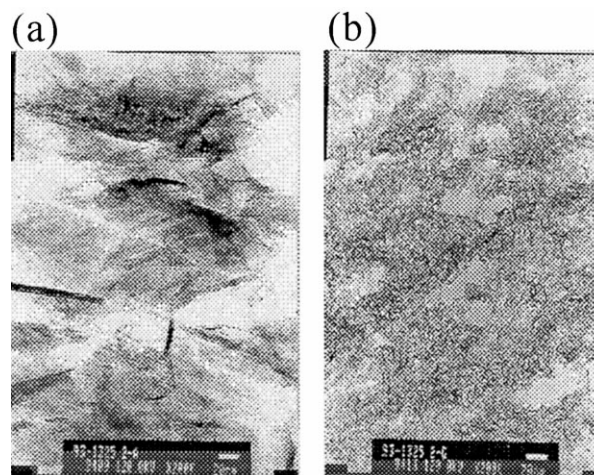

Fig. 1. TEM images of carbon from (a) ''non-oxidized precursor'' and (b) ''oxidized precursor'' with the DMPXG/Py molar ration of 2.0. Heat-treatment temperature was 2800°C.

Table 1
Characteristics of non-graphitizable carbons derived from oxidized COPNA precursors heat-treated at (a) 600°C, (b) 800°C, (c) 1100°C, and (d) 1400°C

DMPXG/Py (molar ratio)	XRD			SG (−)	CI (vol%)	RC (Ah/kg)	IRC$_{1st}$ (Ah/kg)
	D_{002} (nm)	L_c (nm)	L_a (nm)				
(a) HTT: 600°C							
1.0	0.388	1.29	1.17	1.569	58.0	504	318 (41%)
1.5	0.369	1.19	1.17	1.504	62.0	523	307 (39%)
2.0	0.362	1.17	1.10	1.486	64.0	547	254 (34%)
(b) HTT: 800°C							
1.0	0.404	1.14	1.81	1.478	55.1	448	193 (33%)
1.5	0.372	1.07	1.49	1.497	60.0	459	178 (30%)
2.0	0.395	1.04	1.44	1.410	61.3	498	203 (32%)
(c) HTT: 1100°C							
1.0	0.366	1.17	2.32	1.510	54.8	319	107 (27%)
1.5	0.367	1.18	2.31	1.525	54.2	313	107 (28%)
2.0	0.381	1.10	2.17	1.463	56.1	326	116 (28%)
(d) HTT: 1400°C							
1.0	0.367	1.34	3.01	1.513	51.1	226	40 (15%)
1.5	0.360	1.44	2.72	1.538	51.1	238	38 (14%)
2.0	0.375	1.21	2.41	1.442	55.3	213	35 (14%)

Note: SG: specific gravity; CI: cavity index; RC: reversible capacity; IRC$_{1st}$: irreversible capacity at first cycle.

cate that the DMPXG/Py = 1.5 and 2.0 carbons have smaller stacking structure than that of DMPXG/Py = 1.0.

The SI values of DMPXG/Py carbons decreased as the DMPXG/Py molar ratio increased.
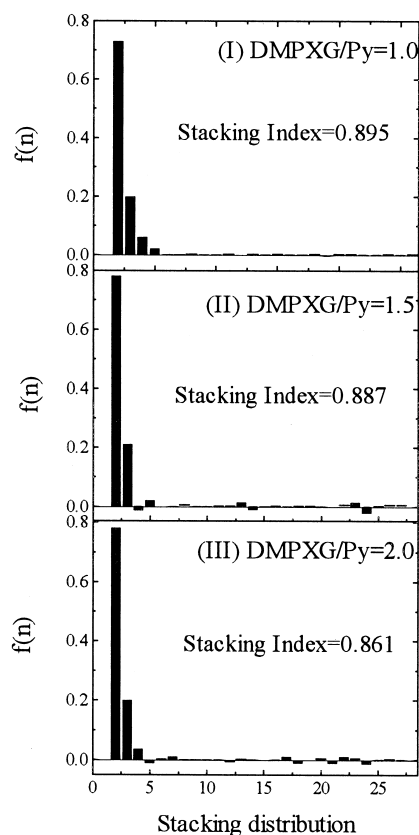

Fig. 2. Structural analyses according to Hirsch's method for non-graphitizable carbons derived from oxidized COPNA precursors: DMPXG/Py molar ratios of (I) 1.0, (II) 1.5, and (III) 2.0.
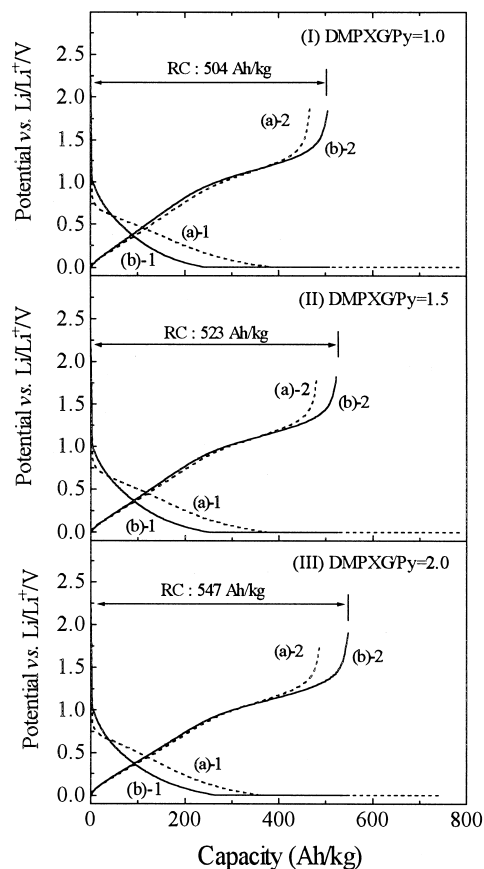

Fig. 3. Charge–discharge profiles of non-graphitizable carbons derived from oxidized COPNA precursors heat-treated at 600°C: DMPXG/Py molar ratios of (I) 1.0, (II) 1.5, and (III) 2.0.
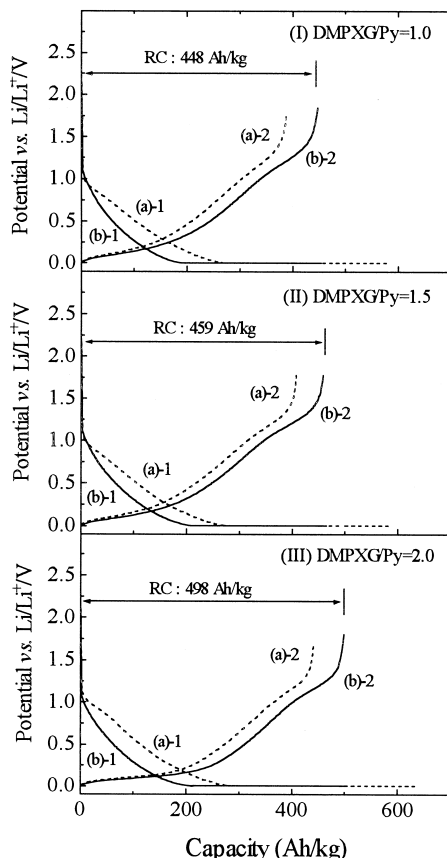
Fig. 4. Charge–discharge profiles of non-graphitizable carbons derived from oxidized COPNA precursors heat-treated at 800°C: DMPXG/Py molar ratios of (I) 1.0, (II) 1.5, and (III) 2.0.

3.2. Anodic performances of carbons

Fig. 3 shows the charge–discharge profiles of the carbon anodes heat-treated at 600°C with a series of DM-PXG/Py molar ratios. In Fig. 3, the first charge and discharge profile (dotted lines) are indicated as (a)-1 and (a)-2, and the reversible charge and discharge profile (solid lines) are shown as (b)-1 and (b)-2), respectively. (These labels are used in the same manner in Figs. 3–5.) At the first charge, the electrolyte decomposition leading to the formation of a passivation layer [34] or solid electrolyte interface (SEI) [35] on the carbon surface was observed around 0.8 V vs. Li/Li$^+$. The irreversible capacity in the first cycle (IRC$_{1st}$ listed in Table 1) decreased with an increase of the CI value. The values in parenthesis in the column of IRC$_{1st}$, which define the retention ratio (as the irreversible capacity normalized to the first charge capacity) also decreased with the CI value. After the second cycle, the electrolyte decomposition reaction was not observed in the charge profile. The discharge capacity gradually increased with cycling, and it reached a constant, reversible capacity (RC), after the fifth cycle. Such phenomenon and correlation were observed with all carbon anodes heat-treated below. Although the reason why the

discharge capacity increased with cycling has not been explained yet, two plausible reasons are thought as follows: (a) the transport of lithium ions through the passivation layer or SEI on the carbon surface improves with cycling; (b) although lithium is first inserted into the irreversible sites, the number of such sites decreased with cycling, resulting in an increase of lithium inserted into reversible sites for 12 h in the charge condition. The present non-graphitizable carbons heat-treated at 600°C had a discharge of plateau regions around 1.0 V vs. Li/Li$^+$.

Fig. 4 shows the charge–discharge profiles of the carbon anodes heat-treated at 800°C with a series of DM-PXG/Py molar ratios. During the first charge, the electrolyte decomposition reaction around 0.8 V vs. Li/Li$^+$ was reduced and there were no significant changes in the IRC$_{1st}$ and efficiency during the first cycle as a function of the molar ratio of cross-linking agent, as compared to those shown in Fig. 2. The IRC$_{1st}$ was suggested the electrolyte decomposition on the carbon surface mainly dominated. The discharge profiles of the carbons heat-treated at 800°C showed two plateau regions around 0.2 and 1.0 V vs. Li/Li$^+$. The increase in the RC with
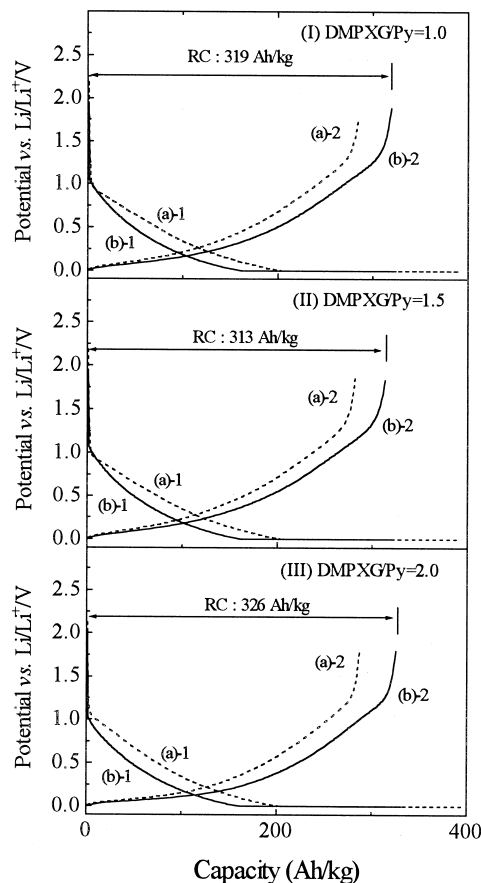

Fig. 5. Charge–discharge profiles of non-graphitizable carbons derived from oxidized COPNA precursors heat-treated at 1100°C: DMPXG/Py molar ratios of (I) 1.0, (II) 1.5, and (III) 2.0.
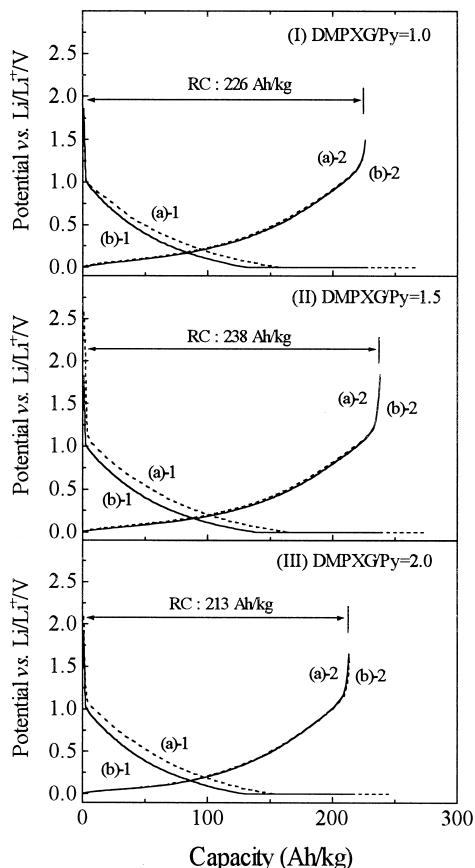
Fig. 6. Charge–discharge profiles of non-graphitizable carbons derived from oxidized COPNA precursors heat-treated at 1400°C: DMPXG/Py molar ratios of (I) 1.0, (II) 1.5, and (III) 2.0.

increasing DMPXG/Py molar ratio essentially corresponded with the increased capacity of the plateau discharge region around 0.2 V vs. Li/Li$^+$. The discharge capacities around 1.0 V vs. Li/Li$^+$ were almost the same regardless of molar ratios.

Fig. 5 shows the charge–discharge profiles of the carbon anodes heat-treated at 1100°C with a series of DMPXG/Py molar ratios. The plateau discharge region around 1.0V vs. Li/Li$^+$ disappeared completely and only the lower plateau discharge region was observable. The CI value of DMPXG/Py = 1.5 carbon was slightly less than that for DMPXG/Py = 1.0 carbon, and, as a result, the discharge capacity decreased.

Fig. 6 shows the charge–discharge profiles of the carbon anodes heat-treated at 1400°C with a series of DMPXG/Py molar ratios. In the first cycles, a smaller amount of electrolyte decomposition reaction was still observed at charging; however, the first discharge profile stayed the same as that after the fifth cycle. In spite of the fact that the CI value increased with an increase in cross-linking agent, there was a tendency for the discharge capacity to decrease as the CI value increased. The charge–discharge properties of non-graphitizable carbons heat-treated above 1400°C are concluded to be dominated by the lithium

intercalation reaction and hence, the discharge capacity decreased as the CI value increased.

4. Discussion

4.1. Correlation among structural parameters

Fig. 7 shows the relationship between various structural parameters of carbons, R, EL, SI, and CI values. Obviously, these parameters are all correlated with CI value as shown in Fig. 7. The parameters R and SI indicate the degree of crystallinity, hence, their decrease reflects the increase of CI value. On the other hand, EL parameter indicates the degree of disorder in the carbon structure, its increase corresponding to the increase of CI value. The parameter R is a facile measure for the amount of mono-layers on the bases of the Hirsch method. However, it suffers a large error when the crystallinity increases. The value of EL gives the edge length of stacking graphene layers, when the crystals in carbon structure are assumed cubic. As the model of CI is based on the graphene layers
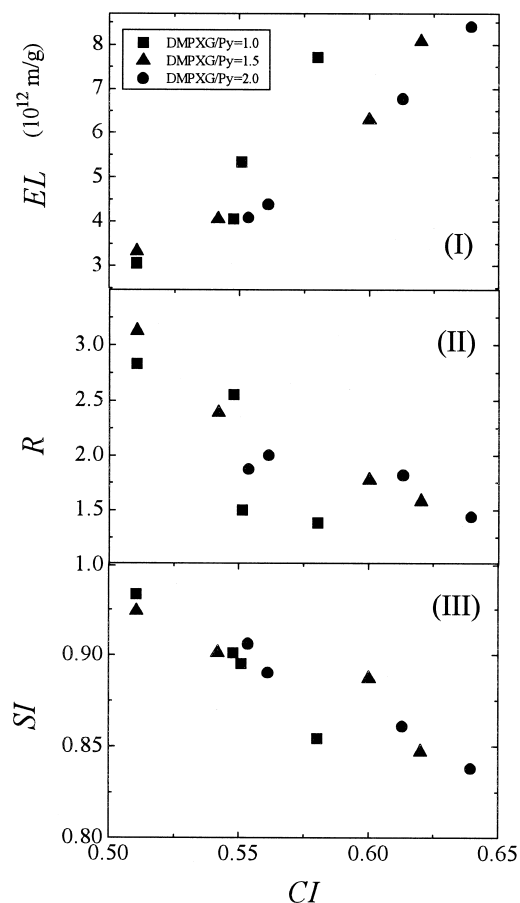

Fig. 7. Relationship among several kinds of carbon structural parameters with different cross-linking agent molar ratios as indicated in the figure: (I) EL, (II) R, and (III) SI as the function of the CI value.

stacked in three dimensions in the carbon structure, the parameter EL could be almost the same parameter of CI in carbon structures. Thus, the CI value is a measure for not only void but also unorganized sites in the carbon, being a comprehensive parameter to characterize the disorder carbon.

4.2. Correlation between capacities and structural parameters

The RC was plotted as a function of the CI values in Fig. 8. The RC increased as the CI value increased, suggesting again that the cavities in the carbons are available for accommodation of lithium species. According to the data in Fig. 5, other structural parameters also show good correlation with the RC, for example, R decreased with an increase in capacity as Xing et al. [36] reported.

The unique characteristic of the CI value is not only to predict the capacity of a carbon, but also to calculate the cavity capacity. A plateau discharge capacity below 0.2 V vs. Li/Li$^+$ could be assumed as "hard-carbon type discharge capacity" and a plateau discharge capacity over 1.0 V vs. Li/Li$^+$ could be assumed as "soft-carbon type discharge capacity". Then, a "total cavity capacity" can be obtained as the sum of these two capacities. Fig. 9 shows the relationship between the total cavity capacity observed by the electrochemical measurements and the theoretical cavity capacity calculated using Eq. (2). The total cavity capacities of the carbons heat-treated below 1100°C showed good correlation with the theoretical capacities of these carbons. However, the deviation of the total cavity capacities of the carbons heat-treated above 1100°C from their theoretical values became increasing. This is because most of the cavities in non-graphitizable

Fig. 9. Relationship between total cavity capacity and theoretical cavity capacity of the non-graphitizable carbons at different heat-treatment temperatures as indicated in the figure.

carbons heat-treated above 1100°C are not suitable for the accommodation of lithium species.

5. Conclusions

Non-graphitizable carbons can be obtained by oxidation graphitizable carbon precursors and the microstructure can be controlled by the extent of cross-linkage which reflects the amount of coupling agent.

The discharge capacities of non-graphitizable carbons derived from DMPXG/Py-based COPNA precursors heat-treated below 1100°C increased with an increase in the CI value. The non-graphitizable carbons heat-treated at 600°C had a plateau discharge region around 1.0 V vs. Li/Li$^+$ and the capacity of the region increased with an increase in cross-linking agent in the same manner as graphitizable carbon materials. The non-graphitizable carbons, heat-treated at 800°C, exhibited completely different discharge profiles from the graphitizable carbons. In particular, the former carbons had two discharge plateau regions at 0.2 and 1.0 V vs. Li/Li$^+$, in contrast, the graphitizable carbons have only one plateau region at 1.0 V. The total discharge capacity depended strongly on the plateau discharge capacity around 0.2 V vs. Li/Li$^+$. This result suggests that the cavities in non-graphitizable carbons are also responsible for the charge–discharge of lithium species. The capacity of non-graphitizable carbons heat-treated above 1100°C has a weak dependence on the cavity volume and this dependence disappears entirely when heat-treated above 1400°C because lithium intercalation between graphene layers became dominant.

Several carbon structural parameters (R, EL, and SI) have strong correlation with the CI value and these parameters also correlate with the discharge capacity. Furthermore, the total cavity capacities of non-graphitizable carbons correlate with the theoretical cavity capacity, as calculated from the CI value. The deviation of the ob-
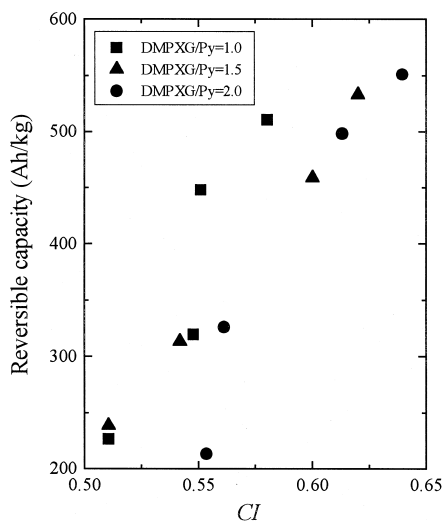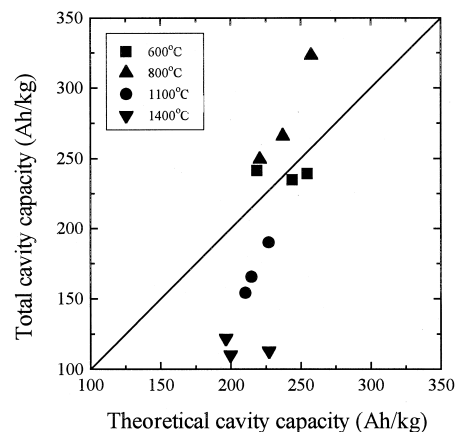

Fig. 8. Relationship between RC of the non-graphitizable carbons with different cross-linking agent molar ratios as indicated in the figure and the CI value.

served capacity from the theoretical cavity capacity of non-graphitizable carbons heat-treated above 1100°C is due to the reduction of the cavities, which are suitable for the accommodation of lithium species.

Acknowledgements

References

[1] M. Lazzari, B. Scrosati, J. Electrochem. Soc. 127 (1980) 773.
[2] B. Di Pietro, M. Patriarca, B. Scrosati, J. Power Sources 8 (1982) 289.
[3] M. Mohri, N. Yanagisawa, Y. Tajima, H. Tanaka, T. Mitate, S. Nakajima, M. Yoshida, Y. Yoshimoto, T. Suzuki, J. Power Sources 26 (1989) 545.
[4] H. Imoto, H. Azuma, A. Omaru, Y. Nishi, in: 58th Meeting of the Electrochemical Society of Japan, Noda,1991, p. 158, Abstract 2F11.
[5] A.K. Sleigh, U. von Sacken, Solid State Ionics 57 (1992) 99.
[6] A. Omaru, H. Azuma, M. Aoki, A. Kita, Y. Nishi, in: The Electrochemical Society Meeting Abstracts, Toronto, ON, Canada, Oct. 11–16 vol. 92-21992, p. 34, Abstract 25.
[7] K. Sato, M. Noguchi, A. Demachi, N. Oki, M. Endo, Science 264 (1994) 556.
[8] S. Yata, H. Kinoshita, M. Komori, N. Ando, T. Kawashimura, T. Harada, K. Tanaka, T. Yamabe, Synth. Met. 62 (1994) 153.
[9] T. Zheng, Q. Zhong, J.R. Dahn, J. Electrochem. Soc. 142 (1995) L211.
[10] T. Zheng, Y. Liu, E.W. Fuller, S. Tseng, U. von Sacken, J.R. Dahn, J. Electrochem. Soc. 142 (1995) 2581.
[11] Y. Liu, J.S. Xue, T. Zheng, J.R. Dahn, Carbon 34 (1996) 193.
[12] R. Yazami, M. Deschamps, in: The Electrochemical Society Extended Abstracts, Miami Beach, Florida, Oct. 9–14 vol. 94-21994, p. 148, Abstract 94.
[13] Y. Matsumura, S. Wang, J. Mondori, Carbon 33 (1995) 1457.
[14] H. Xiang, S. Fang, Y. Jiang, J. Electrochem. Soc. 144 (1997) L187.
[15] K. Tokumitsu, A. Mabuchi, H. Fujimoto, T. Kasuh, J. Power Sources 54 (1995) 444.
[16] A. Mabuchi, K. Tokumitsu, H. Fujimoto, T. Kasuh, J. Electrochem. Soc. 142 (1995) 1041.
[17] A. Mabuchi, K. Tokumitsu, H. Fujimoto, T. Kasuh, J. Electrochem. Soc. 142 (1995) 3049.
[18] K. Tokumitsu, A. Mabuchi, H. Fujimoto, T. Kasuh, J. Electrochem. Soc. 143 (1996) 2235.
[19] W. Xing, J. Xue, J.R. Dahn, J. Electrochem. Soc. 143 (1996) 3047.
[20] S. Otani, Carbon 3 (1965) 31.
[21] S. Otani, Carbon 5 (1967) 219.
[22] I. Mochida, T. Inaba, Y. Korai, H. Fujitsu, K. Takeshita, Carbon 21 (1983) 543.
[23] I. Mochida, T. Inaba, Y. Korai, K. Takeshita, Carbon 21 (1983) 553.
[24] S. Otani, A. Oya, Kogyokagakukai-shi 73 (1970) 493.
[25] T. Maeda, S.M. Zeng, K. Tokumitsu, J. Mondori, I. Mochida, Carbon 31 (1993) 407.
[26] H. Fujimoto, A. Mabuchi, K. Tokumitsu, T. Kasuh, Carbon 32 (1994) 1249.
[27] R. Diamond, PhD Thesis, University of Cambridge, 1956.
[28] R. Diamond, Acta Cryst. 10 (1957) 359.
[29] R. Diamond, Acta Cryst. 11 (1958) 129.
[30] R. Diamond, Philos. Trans. R. Soc. London, A 252 (1960) 193.
[31] P.B. Hirsch, Proc. R. Soc. (London), A 226 (1954) 143.
[32] M. Shiraishi, Y. Sanada, Nippon Kagakukai-shi 1 (1976) 153.
[33] K. Tokumitsu, H. Fujimoto, A. Mabuchi, T. Kasuh, Carbon 37 (1999) 1599.
[34] R. Fong, U. von Sacken, J.R. Dahn, J. Electrochem. Soc. 137 (1990) 2009.
[35] E. Peled, C. Menachem, D. Bar-Tow, A. Melman, J. Electrochem. Soc. 143 (1996) L4.
[36] W. Xing, J. Xue, T. Zheng, A. Gibaud, J.R. Dahn, J. Electrochem. Soc. 143 (1996) 3482.